ELSEVIER

Chemical Engineering Journal 129 (2007) 1–10

Chemical Engineering Journal

www.elsevier.com/locate/cej

Effect of the catalyst properties on the performance of a reverse flow reactor for methane combustion in lean mixtures

Miguel A.G. Hevia, Salvador Ordóñez *, Fernando V. Díez

Department of Chemical and Environmental Engineering, University of Oviedo, Julián Clavería 8, 33006 Oviedo, Spain

Received 11 August 2006; received in revised form 15 October 2006; accepted 26 October 2006

Abstract

This paper analyses the role of the catalyst properties (specially the different activities and thermal stabilities of the studied catalysts) on the performance of reverse flow reactors (RFR) for the combustion of lean methane-air mixtures. Two different γ-Al_2O_3-supported industrial catalysts have been selected as representatives of the two types of catalysts used in these processes: metal oxides (mainly Mn oxide) and noble metals based (Pd) catalysts. The different activities and stabilities of these catalysts (Pd is more active but undergoes thermal deactivation) largely affect the operation of the RFR. The implications of these differences are comprehensively studied using both numerical simulation (considering an heterogeneous one-dimensional model), and a bench scale RFR featuring a novel temperature control system that allows an instantaneous compensation of heat losses, obtaining a performance similar to that expected for larger industrial scale units. Therefore, it is concluded that the catalyst selection, which depends mainly on the nature of the emissions to be treated, largely affects the main operation variables to be fixed in order to obtain a stable and autothermal operation in a RFR, i.e. preheating temperature, inlet concentration and switching time.

Keywords: Reverse-flow reactor; Afterburner; Pd-catalysts; Metal oxide catalysts

1. Introduction

Reverse flow reactors (RFR) are one of the most studied transient-operating reactors in the last decades. A RFR is a packed bed reactor in which the feed flow direction is periodically reversed. Therefore, when an exothermic reaction is conducted in a RFR, it traps a hot zone in the reactor. This enables a self-maintained operation at high temperatures, even for feeds having a low adiabatic temperature rise, as in the case of the methane-air lean mixtures.

RFR have normally sections of inert material at both ends of the bed mainly intended to keep the high temperature wave far from the limits of the bed. RFR have been widely regarded as the most promising forced unsteady-state catalytic reactors since they were proposed by Matros and co-worker [1] in the seventies, and later on industrially applied to the oxidation of SO_2. RFR have been proposed for other reversible processes like methanol synthesis [2] because the periodic flow reversal makes possible to have a bell-shaped temperature profile in the reactor, very suitable for maximizing the yield of reversible reactions. Other processes for which RFR have been proposed to are synthesis gas production [3,4], production of phtallic anhydride from *o*-xylene [5], selective catalytic reduction (SCR) of NO_x [6,7], and endothermic reactions with heat regeneration by vapour [8] or by coupled exothermic reactions [9,10].

The abatement of lean hydrocarbon mixtures in air by catalytic combustion in RFR has been much more widely investigated than the other aforementioned applications. Furthermore, these reactions are, besides the SO_2 oxidation and the SCR of NO_x, the only reactions that, by 1996, had already been industrially applied [11]. Nowadays RFR continue being proposed to new hydrocarbon abatement applications like the tail gas of the ventilation systems of coal mines, which has nowadays become into a great environmental problem because of the Kyoto Protocol directives [12,13].

As indicated previously, the flow reversal allows both the auto-ignition of the system from an initial preheated state and the maintenance of an equilibrated energy balance once the periodic steady state (PSS) is reached. It has been stated that

Abbreviations: GWP_{20}, global warming potential in a 20-year basis; ODE, ordinary differential equations; PDE, partial differential equations; PSS, periodic steady state; RFR, reverse-flow reactor; SCR, selective catalytic reduction; VOC, volatile organic compounds

* Corresponding author. Fax: +34 985 103 434.
E-mail address: sordonez@uniovi.es (S. Ordóñez).

1385-8947/$ – see front matter © 2006 Elsevier B.V. All rights reserved.
doi:10.1016/j.cej.2006.10.028

Nomenclature

a	external particle surface area per unit volume of reactor (m^{-1})
C_p	specific heat at constant pressure ($J\,kg^{-1}\,K^{-1}$)
d_P	pellet diameter (m)
d_W	wall thickness (m)
D_{eff}	effective mass dispersion coefficient ($m^2\,s^{-1}$)
D_R	reactor inner diameter (m)
E_a	activation energy ($J\,kmol^{-1}$)
h	gas-solid heat transfer coefficient ($J\,m^{-2}\,K^{-1}\,s^{-1}$)
ΔH_c	enthalpy of combustion ($J\,mol^{-1}$)
k_∞	pre-exponential factor (s^{-1})
k_{eff}	effective heat dispersion coefficient ($J\,m^{-1}\,K^{-1}\,s^{-1}$)
K_G	gas-solid mass transfer coefficient ($m\,s^{-1}$)
M	molecular weight of the gas mixture ($g\,mol^{-1}$)
L	Length of the reactor (m)
L_b	Length of the bed (m)
L_i	Length of the inert layer section (m)
R	ideal gas constant ($J\,K^{-1}\,mol^{-1}$)
t	time (s)
t_c	switching time (s)
T	temperature (K)
ΔT_{ad}	adiabatic temperature rise (K)
u	surface velocity ($m\,s^{-1}$)
v	interstitial velocity ($m\,s^{-1}$)
x	axial reactor coordinate (m)
y	molar fraction
$y_{G,out}$	molar fraction at the outlet of the reactor
$y_{G,out,av}$	molar fraction at the outlet of reactor, averaged during a semicycle, without considering the *blow-up*

Greek symbols

ε	bed void fraction
η	intraparticle effectiveness factor
λ	thermal conductivity ($J\,m^{-1}\,K^{-1}\,s^{-1}$)
ρ	density (or apparent density for the catalyst) ($kg\,m^{-3}$)

Subscripts and superscripts

0	inlet conditions (pressure 1.013×10^5 Pa)
ext	external property
eff	effective value
G	gas phase
i	inert material
max	maximum
rel	relative value (to the maximum one)
S	solid phase or solid surface
W	reactor wall

auto-thermal operation is possible in RFR with ΔT_{ad} as low as 10 K [14], whereas in recuperative processes (conventional fixed bed reactors with heat-exchangers downstream) the minimum ΔT_{ad} required is about 150 K [15]. Recuperative processes tend to extinction easily under temporary falls of the VOC concentration or variations of the gas feed flow, while RFR are able to keep the ignited state even under important gas flow and concentration perturbations [16].

Due to these advantages for the combustion of lean hydrocarbon-air mixtures, RFR reactors were widely studied for these processes in the recent years, both experimentally and, to a larger extent, by numerical simulation. Therefore, the relationships of the reactor performance with the operating conditions and the physical properties of the inert packing and catalyst are well known.

So, Eigenberger and Nieken [17] showed that maximum temperature in the reactor increases as the volumetric fraction of the inert ends increases. In binary mixtures of VOCs, it is possible to have a partially ignited state in which the most refractory compound to combustion is not burned if its concentration is not high enough for self-sustaining the process [18]. Similar conclusions were obtained by Vandebeld and Westerterp [19,20], also finding that pressure hardly affects the performance of the process provided that the inlet mass flow is constant and the deep oxidation kinetics of the involved compounds fit well to a first order law. Sapundzhiev et al. [21] showed in a simulation study that the maximum temperature of the reactor and its stability increase as the heat capacity of the inert packing increases. They also studied experimentally the catalytic combustion of methane lean mixtures finding a good fitting to a heterogeneous bidimensional model [22], and they proposed and simulated a new RFR type in which there is a heat exchanger in the centre of the catalytic section [23]. Barresi and co-workers have published several papers on the modelling and simulation of RFR applied to combustion of lean VOC mixtures, studying relevant aspects like the response to periodic variations in the feed gas flow and concentration [16], the behaviour during the transient start-up before reaching the PSS [24], or the control of the flow reversals depending upon instant temperature measurements inside the bed [25]. Most recent works are predominantly theoretical, dealing with model refinements and simulations aimed at the proposal of innovative and robust control systems [26,27]; and at optimizing the reactor structure [28], and the heat recovery systems [29].

In our previous works, we have proposed and successfully tested an innovative temperature control system which dynamically compensates the heat losses of small-medium sized research RFR, overcoming the typical heat losses gap in the up-scale of these systems [30]. The effect of the wall thermal properties on the reactor performance was also exhaustively studied, concluding that this effect is increasingly important as the surface velocity decreases [31]. We have also proposed a novel model predictive control system for RFR that allows avoiding both the extinction and an overheating of the catalyst by changing the switching time of the flow reversal [32], and we have compared the performance of packed bed and structured bed RFR [33].

This paper is focused on an aspect that has not been examined comprehensively so far: the role of catalyst properties, particularly the catalyst activity and its resistance to thermal ageing. The few works dealing with the influence of the catalyst properties on the reactor performance are only focused on the physical properties of the catalyst [34], reporting in several cases an inverse relationship between catalyst activity and maximum temperature [14,17,18]. In this work, the implications of the catalyst activity and the resistance to thermal deactivation for both reactor performance and operating conditions are determined. This topic is very relevant because two different types of catalysts are used in the catalytic abatement of lean hydrocarbon emissions: noble metal based and metal oxides based, which in turn lead to important differences in the reactor performance. Noble metal catalysts are highly active and lowly thermal resistant whereas the opposite behaviour is found for the metal oxides catalysts. Basically, operation with noble metal catalysts require less temperature and therefore the energy consumption and the heat loses are lower, but metal oxides catalysts resist higher temperatures without risk of deactivation, and then they can operate with higher VOC concentrations. It must be also considered that the presence of different impurities in the off-gases to be treated (especially sulphur compounds) can lead to the use of metal oxide catalysts, also less sensitive to sulphur poisoning [35].

As the present work is focused on the study of the effect of the different activity of the selected catalysts, we try to use catalysts with similar physical properties. By this reason, two γ-Al_2O_3-supported catalysts were selected, the active phase (palladium or manganese oxide) being the only significant difference between them. The reaction studied is the combustion of methane because it is a good model compound since it is more refractory to catalytic combustion than most hydrocarbons. Furthermore, methane abatement is interesting by itself because it is the most largely emitted hydrocarbon (coke ovens, coal mines venting systems, composting facilities, manure management, etc.) and the global warming potential (GWP_{20}) of the resulting combusted emissions (CO_2) is about sixty times lower.

2. Modelling and dynamic simulations

As it was demonstrated in previous papers [30–32] a heterogeneous one-dimensional model is accurate enough for describing the behaviour of the reverse flow reactor studied in this work. Radial profiles of temperature and concentrations are negligible because of the relatively low diameter of the reactor (very small radial Biot number). Concerning to the number of phases taken into account, a heterogeneous model (consider balances to both gas and solid phase) has been used since it is accepted to be more accurate for highly exothermic reactions at unsteady state [20]. Pressure losses through the reactor were neglected and plug flow, with dispersive transport of mass and energy, was assumed for the gas phase; ideal gas law being used. The transient term was taken into account in the gas phase equations and in the energy equation for the solid phase, while pseudo-steady state was assumed for the balance to the solid catalytic surface. The effect of the intraparticle mass transport was included in the model by means of the effectiveness factor.

For the particular case studied in this work, that is one active component (methane), first order kinetics, and adiabatic reactor, the set of partial differential-algebraic equations PDAE can be written as shown in Eqs. (1)–(5). As previously stated by other authors like Vandebeld and Westerterp [20], the effect of the reactor wall in the energy balances of the system is taken into account through a term corresponding to the heat transfer between the gas phase and the wall. A more general model, regarding the kinetics, number of reagents, and for non-negligible heat exchange between the reactor and the environment, can be found in a previous work [30], where the correlations used to calculate the heat and mass transfer parameters appearing in the model are also included.

- Gas phase energy balance

$$\frac{\partial T_G}{\partial t} = -v\frac{\rho_{G,0}}{\rho_G}\frac{\partial T_G}{\partial x} + \frac{k_{eff}}{C_{p,G}\rho_G}\frac{\partial^2 T_G}{\partial x^2} + \frac{ha}{C_{p,G}\rho_G\varepsilon}(T_S - T_G) - \frac{4h_W}{C_{p,G}\rho_G D_R\varepsilon}(T_G - T_W) \quad (1)$$

- Solid phase energy balance

$$\frac{\partial T_S}{\partial t} = \frac{\lambda_{S,eff}}{C_{p,S}\rho_S}\frac{\partial^2 T_S}{\partial x^2} + \frac{K_G a(-\Delta H_c)\rho_G}{C_{p,S}\rho_S(1-\varepsilon)M}(y_G - y_S) - \frac{ha}{C_{p,S}\rho_G(1-\varepsilon)}(T_S - T_G) \quad (2)$$

- Energy balance to the reactor wall

$$\frac{\partial T_W}{\partial t} = \frac{\lambda_W}{C_{p,W}\rho_W}\frac{\partial^2 T_W}{\partial x^2} + \frac{D_R h_W(T_G - T_W) - (D_R + 2d_W)h_{ext}(T_W - T_{ext})}{C_{p,W}\rho_W d_W(D_R + d_W)} \quad (3)$$

- Gas phase mass balance

$$\frac{\partial y_G}{\partial t} = -v\frac{\rho_{G,0}}{\rho_G}\frac{\partial y_G}{\partial x} + D_{eff}\frac{\partial^2 y_G}{\partial x^2} + \frac{K_G a}{\varepsilon}(y_S - y_G) \quad (4)$$

- Solid phase mass balance

$$K_G a(y_G - y_S) = (1-\varepsilon)\eta k_\infty \exp(-E_a/RT_S)y_S \quad \text{(1st order kinetics)}$$

$$K_G a(y_G - y_S) = 0 \quad \text{in the inert sections} \quad (5)$$

A Fortran code has been used to perform the dynamic simulations. The PDE system is transformed into a set of ODE by the discretization of the reactor length into a grid of 101 equidistant points. The resulting ODE system is integrated by a Fortran commercial routine implemented in the code and called LSODES, which belongs to the package ODEPACK [36].

3. Experimental set-up

The high external surface to volume ratios of small sized tubular reactors makes the heat losses to have a significant influence in the system in comparison to larger industrial units, where the performance is essentially adiabatic. Therefore, an important gap in the up-scale is generated by the non-adiabatic behaviour of small-scale research units. We have proposed and patented [37] an innovative temperature control system which allows compensating the heat losses, thus obtaining a nearly-adiabatic behaviour. The components of that control system and of the rest of the RFR unit used for the experiments are shown in the flow diagram of Fig. 1 and listed in its caption. The idea consists basically of an oven surrounding the tubular reactor, axially divided in independent sections or band heaters (14), each one with its own temperature control system involving a temperature measurement (thermocouple), a heating system (electric resistances), and a PID controller. The set-point for the controllers is the temperature measured inside the reactor in an axial position corresponding to the centre of the section. A blower (17) makes cooling air circulating inside the band heaters in order to remove heat fast enough when the temperature inside the reactor is decreasing. This system allows virtually eliminating the driving force for the heat transfer between the reactor and its surroundings, but maintaining the typical steep axial temperature profile of RFR performing exothermic reactions. A further description of the band heaters design and of the control system is available in a previous paper [30], and the experimental results showing the closeness of this system to adiabatic performance are also available in recent works [30–32] and confirmed in the results reported in this paper.

The reactor is a stainless steel cylinder 0.8 m long, with a bed length of 0.5 m, and with an internal diameter of 0.05 m (16). The reaction blends (methane diluted in air) were made up

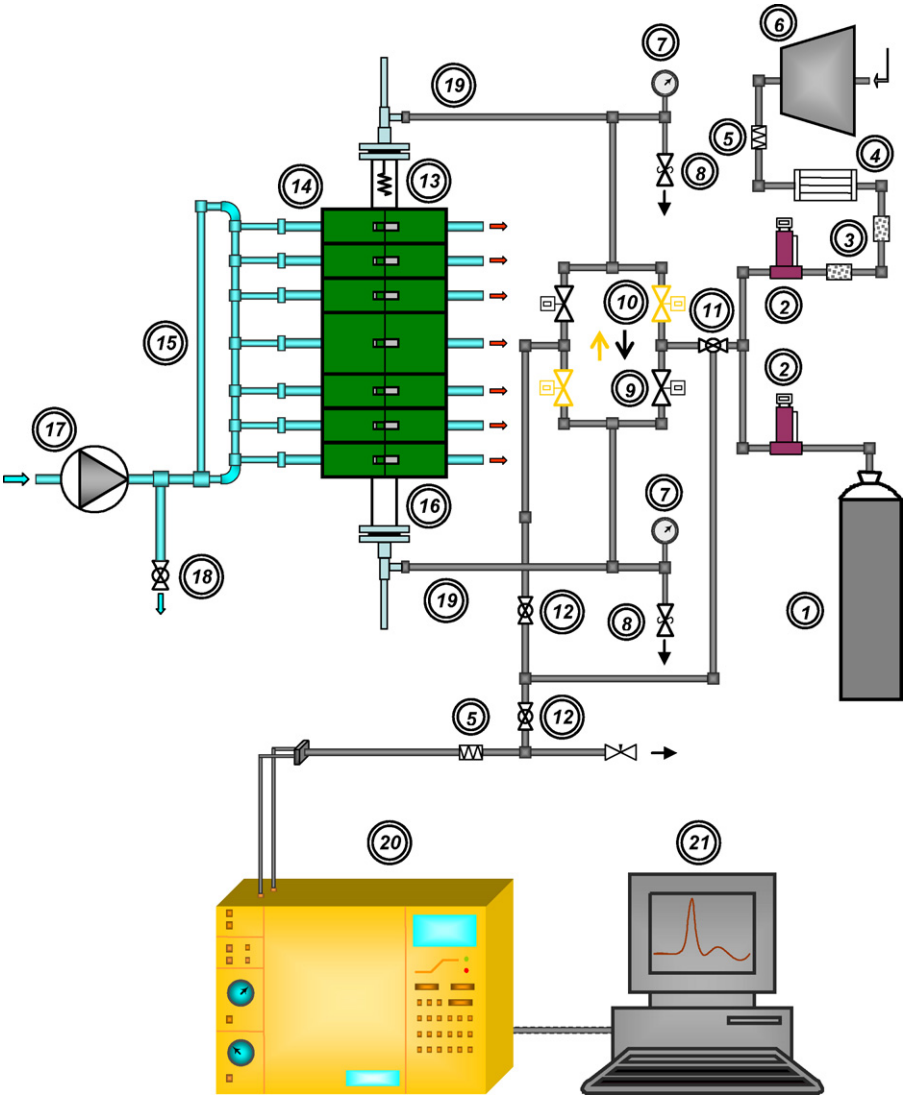

Fig. 1. Flow diagram of the experimental apparatus: (1) Synthetic mixture air/CH_4; (2) Mass-flow controllers; (3) Oil filters; (4) Cooling dryer; (5) Particles filter; (6) Compressor; (7) Pressure gauges; (8) Relief valves; (9) Solenoid valves (downward flow when closed); (10) Solenoid valves (upward flow when closed); (11) Body valve (three-way); (12) Body valve (one way); (13) Preheater; (14) Modular oven; (15) Distribution of cooling air; (16) Reactor; (17) Blower; (18) Body valve (regulation); (19) Flexible tubing; (20) Gas cromatograph; (21) Computer.

by mixing two gas streams controlled by mass flow regulators (2). One was air duly filtered (3 and 5) and dried (4) coming from a compressor (6), and the other one was a mixture of 2.5% vol. methane in synthetic air from a gas cylinder (1). A three-way valve (11), downstream the mixing point, allows bypassing the gaseous feed directly to the GC (20). Two pairs of solenoid valves (9 and 10), electrically coupled in diagonal as they appear in Fig. 1, allow accomplishing the flow reversals.

Two commercial sphere-shaped γ-alumina-supported catalysts have been used, representing each one the group of metal oxides catalysts and noble metal catalysts. The first one shaped in spheres of 0.004 m diameter, the active phase being a non-stoichiometric metal oxide (Mn), whereas the second one consisted of spheres of 0.002–0.004 m diameter, Pd (0.72 wt.%) being the active phase. Catalysts were supplied by Haldor-Topsoe and BASF, respectively. Kinetics of methane combustion over these catalysts had been previously studied using a lab-scale fixed bed isothermal reactor and a methodology described elsewhere [38]. A pseudo-first order model was proven to be accurate enough to describe the kinetics of methane combustion over these catalysts [39]. The kinetic parameters obtained are shown in Table 1.

Glass spheres of 0.004 m diameter were used as inert material in the bed. For the batches with the metal oxides catalyst, the bed consisted of two inert sections at both ends of 0.13 m each, and a central one of 0.24 m filled with catalyst particles. For the Pd catalyst the lengths distribution of the sections was the same, but the central one consisted of a mixture of catalyst particles and glass spheres. Otherwise, all the reactant would be converted in a very short length of the active section due to the high activity of the Pd catalyst, and an important part of it would have been misused. An alternative solution could have been to shorten the catalytic section, and therefore to enlarge the inert sections. Nevertheless, this option is inconvenient. Firstly, because of the comparison between catalysts losses validity if the volumetric ratio of inert/active section changes; and secondly because volumetric fractions higher than 50% are not common. Finally, a too short catalytic section leads to a very narrow space for the high temperature wave to move inside the active section, becoming the system more prone to extinction at high switching times.

Table 1
Main operation conditions and physical properties of the materials used in this work

Properties of the catalyst (Pd/metal oxides)	
Pellet diameter (spheres), d_P (m)	0.002–0.004/0.004
Density (apparent), ρ_S (kg m^{-3})	1257/1541
Specific heat, $C_{p,S}$ (J kg^{-1} K^{-1})	836/836
Inner porosity	0.519/0.451
Tortuosity	2/2
Thermal conductivity, λ (W m^{-1} K^{-1})	0.042/0.042
Bed void fraction, ε	0.36/0.36
Pre-exponential factor, k_∞ (s^{-1})	1.58×10^{11}/2.71×10^{9}
Activation energy, E_a (J mol^{-1})	1.13×10^{5}/1.22×10^{5}
Properties of the bed inert material (glass)	
Diameter (spheres), d_P (m)	0.004
Density, $\rho_{S,i}$ (kg m^{-3})	2590
Specific heat, $C_{p,i}$ (J kg^{-1} K^{-1})	836
Thermal conductivity, λ_i (W m^{-1} K^{-1})	0.65
Inert layers volumetric fraction	0.52
Operating conditions (Pd/metal oxides)	
Surface velocity, u_0 (m s^{-1})	0.155/0.143
Preheating temperature, $T_{S,0}$	624–633/669–683
Inlet gas temperature, $T_{G,0}$ (K)	303/315
Inlet concentration, $y_{G,0} \times 10^6$	2500/3500
WHSV (h^{-1})	12.5/2.36
t_c (s)	150–600/150–600
Reactor (stainless steel)	
Density, ρ_S (kg m^{-3})	7700
Specific heat, $C_{p,W}$ (J kg^{-1} K^{-1})	500
Thermal conductivity, λ_W (W m^{-1} K^{-1})	19.51
Wall thickness, d_W (m)	1.15×10^{-3}

4. Results and discussion

4.1. Comparison of the stability interval and catalytic bed maximum temperature

The performance of a RFR for the combustion of lean mixtures depends on different factors. Some of them are properties of the off-gases to be treated, such as the hydrocarbon concentration or the flow rate. Other must be fixed for a given reactor, such as the preheating temperature or the surface velocity (which will depend on flow rate and reactor dimensions), not being commonly changed during the operation. By contrast, the switching frequency could be easily varied depending on the conditions of the feed.

Concerning to the operating conditions to be fixed, the three main parameters to be considered are: the autothermal operation of the reactor, the maximum temperature reached in the catalytic bed (which can affect the thermal stability of the catalyst), and the concentration of unconverted hydrocarbons in the reactor outlet because of kinetic and *blow-up* effects (the last effect depends only on the switching time and reactor conformation).

The two main differences between the metal oxides and noble metal catalysts are the activity and the thermal ageing threshold. The former are less active, but more resistant to thermal deactivation than the latter. In the case of the metal oxides catalyst used in this work, it was tested, in the same reactor of the kinetic experiments, that it is necessary to work with temperatures below 923 K in order to ensure the absence of thermal deactivation, whereas for the Pd catalyst; the maximum allowable temperature is of 773 K. The higher thermal resistance of the metal oxides catalyst confers it the capability of working with fuel-richer mixtures. On the other hand, the higher activity of the Pd catalyst makes possible to work with lower temperatures and to obtain self-maintained operation with lower values of initial concentration ($y_{G,0}$). Taking into account the two aforementioned factors governing the workable $y_{G,0}$ intervals (thermal resistance and minimum $y_{G,0}$), metal oxide catalysts are suitable for higher values of $y_{G,0}$ than noble metal catalysts do.

Concerning to their performance on the reverse flow reactor, the stability intervals for both kind of catalysts are shown in Fig. 2. As observed, the Pd catalyst shows wider stability inter-

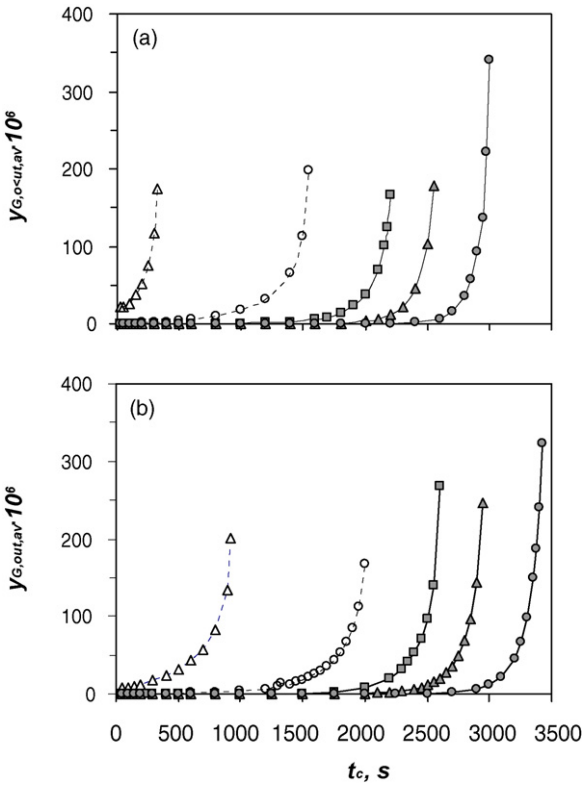

Fig. 2. Outlet methane concentration (averaged during a semicycle) vs. switching time in the PSS for the metal oxides (a) and Pd (b) catalysts: $y_{G,0} \times 10^6 = 5000$ (continuous line, ●); $y_{G,0} \times 10^6 = 4000$ (continuous line, ▲); $y_{G,0} \times 10^6 = 3500$ (continuous line, ■); $y_{G,0} \times 10^6 = 3000$ (discontinuous line, ○); $y_{G,0} \times 10^6 = 2500$ (discontinuous line, △).

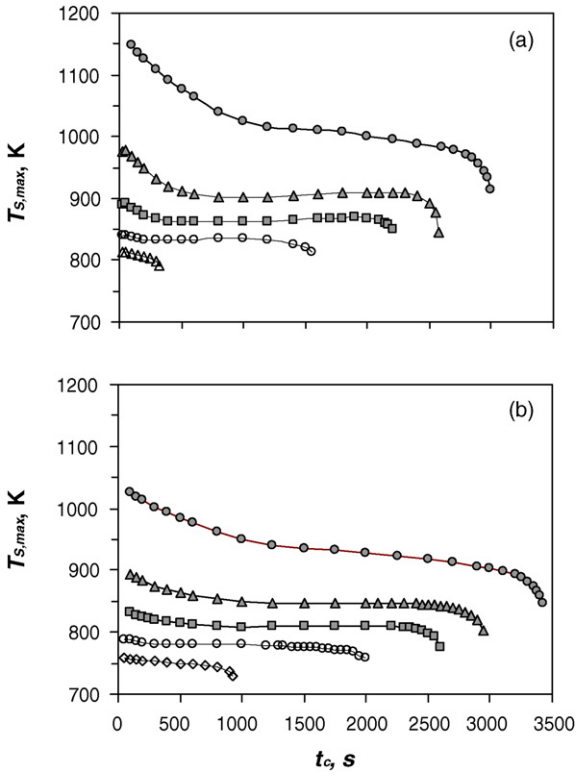

Fig. 3. Maximum solid temperature vs. switching time in the PSS for the metal oxides (a) and Pd (b) catalysts: $y_{G,0} \times 10^6 = 5000$ (continuous line, ●); $y_{G,0} \times 10^6 = 4000$ (continuous line, ▲); $y_{G,0} \times 10^6 = 3500$ (continuous line, ■); $y_{G,0} \times 10^6 = 3000$ (discontinuous line, ○); $y_{G,0} \times 10^6 = 2500$ (discontinuous line, △).

vals than the metal oxide catalyst (for a given $y_{G,0}$, the former is able to provide full conversion for higher t_c). This is caused by the higher activity of the catalyst, which allows autothermal operation with lower values of $y_{G,0}$ and higher switching times. From this point of view, the performance of the Pd catalyst is better since both the reactor is able to deal with lower hydrocarbon concentrations, and the robustness of the system is improved.

It is not so straightforward to withdraw conclusions from the point of view of the maximum temperature reached in the reactor. On the one hand, the reactor operates at higher temperatures when using the metal oxides catalyst, increasing these temperatures as the methane concentration increases (Fig. 3). However, as previously mentioned, the main effect of this parameter is related to the thermal stability of the catalyst, being the metal oxide catalyst more resistant to thermal deactivation.

The results can be expressed in terms of stability regions; that is, in terms of the switching time (t_c) interval that leads to stable auto-thermal operation for every $y_{G,0}$. So, for a given gas velocity (u_0), there is a region of the map $y_{G,0}$ versus t_c which leads to satisfactory operation, considering satisfactory operation as that with a PSS maximum temperature of the catalytic bed ($T_{S,max}$) and average methane outlet concentration ($y_{G,out,av}$) below certain pre-established thresholds. The threshold for $T_{S,max}$ is normally given by the maximum allowable temperature of the catalyst, whereas the threshold for $y_{G,out,av}$ depends on the nature and the scope of the process. For instance, in the exhaust gases abatement processes, the maximum concentration of the pollutant at the outlet depends normally on environmental regulations. These maps, can be used to develop a model predictive control system which acts over t_c in order to keep the system below the desired values of $T_{S,max}$ and a $y_{G,out,av}$ under $y_{G,0}$ perturbations, being also applicable to u_0 perturbations, if a map of u_0 versus t_c is used instead [32]. Fig. 4 shows the stable operation regions in the $y_{G,0}$ versus t_c plot for the two catalysts used in this work (considering the above-mentioned differences on the maximum temperature), obtained by simulations in which they were used the physical properties and kinetic parameters contained in Table 1. Values of t_c lower than 100 s have been not considered in order to avoid the conditions at which the *blow-up* effects are more important, as it will be discussed later.

Two lines limit stability regions: an upper one, above which the maximum temperature of the catalytic bed is higher than that allowed for avoiding thermal deactivation, and a bottom one, below which the outlet methane concentration is higher than required. As a general trend, for a given value of $y_{G,0}$, the maximum workable t_c is higher for the Pd catalyst. For example, for $y_{G,0} = 3000$ and $y_{G,out,av} = 100$ ppm, it is possible to operate with a t_c up to 1900 s for the Pd catalyst, whereas for the metal oxides that upper limit is of 1475 s. As switching time increases, the cold front originated by the feeding of room temperature gas gets longer. Above a certain value of t_c the temperature

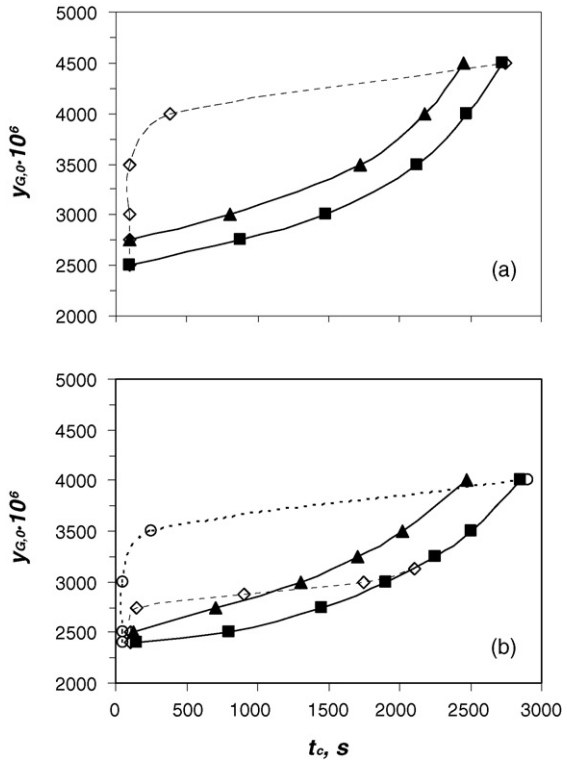

Fig. 4. Operation regions for the metal oxides (a) and Pd (b) catalysts ($u_0 = 0.143\ m\ s^{-1}$). Operation above the upper lines (discontinuous line, ◊) leads to $T_{S,max}$ higher than 923 K (chart (a)) and 773 K (chart (b)). Operation below the lower lines leads to $y_{G,out}$ higher than 10 ppm (continuous line, ▲) and 100 ppm (continuous line, ■). Chart (b) includes also an upper line for a hypothetical catalyst identical to the Pd one but with an allowable $T_{S,max}$ 50 K higher (discontinuous line, ◯).

of the gas entering the catalytic section and therefore the temperature of the catalyst in that zone starts to decrease. The Pd catalyst, due to its lower ignition temperature and activation energy, admits higher temperature falls without having noticeable consequences in the conversion, and therefore, for a given $y_{G,0}$, its maximum workable t_c is higher. However, the area of the workable region is remarkably smaller for the Pd catalyst. That is because the $y_{G,0}$ workable window is highly constrained due to its relatively low maximum allowable temperature (773 K compared to 923 K for the metal oxides catalyst). In general, the conclusion is that higher catalytic activities lead to higher maximum workable t_c, while higher thermal resistances lead to higher maximum workable $y_{G,0}$, the effect of the latter being more marked for the properties of the catalysts studied in this paper.

It is worth to point out that these stability regions are expected to be larger for less refractory compounds than methane, because the corresponding ignition temperatures are lower, and therefore, the admissible temperature rise margins are higher. Furthermore, in the case of the of the Pd catalyst, there are a number of studies which have shown that it is possible to improve the thermal stability of the catalyst, for instance changing the support (γ-Al_2O_3) by ZrO_2, obtaining activities even higher [40]. Therefore, it should be considered that it is possible to find palladium catalysts more resistant to thermal deactivation. An allowable $T_{S,max}$ just 50 K higher (823 K) would lead to a remarkable enlargement of the stability region, and therefore of the robustness of the RFR under $y_{G,0}$ perturbations, as shown in Fig. 4 (chart b).

4.2. Influence of preheating on the catalyst performance

The value of the preheating temperature ($T_{S,0}$) must be high enough to ensure the auto-ignition of the reactor. It is necessary a certain initial conversion in order to produce heat from the very beginning of the operation, leading to a net favourable balance of energy for the reactor during the start-up. As a consequence, the minimum required $T_{S,0}$ decreases as the catalytic activity increases. The $T_{S,0}$ used in this work for the Pd catalyst leads to full conversion from the beginning, while that used for the metal oxides catalyst, in spite of being about 50 K higher, leads to a partial escape of methane which decreases as the start-up develops evolving toward higher temperatures in the catalytic section. In spite of the initial pollutant escape, the relatively low $T_{S,0}$ values have some advantages. Namely, they allow saving energy in the preheating operation, and they provide a fast way of detecting catalyst deactivation just by checking whether the initial $y_{G,out}$ remains constant every time the rector is started-up with the same operating conditions, particularly $T_{S,0}$.

4.3. Evaluation of the catalyst performance in terms of unconverted hydrocarbon emissions (blow-up)

In addition to the reactor extinction and the maximum temperature of the catalytic bed, the switching time also determines the fraction of the off-gases that leave the system without being converted. This effect is known as *blow-up* or *wash-out* [41] and consists in the instant escape of gases without converting that takes place during the flow reversals. This effect can be nowadays eliminated by means of three bed RFR configurations, which are being increasingly used in new installations [42]. The *blow-up* effects are more important at high switching frequencies. The magnitude of this effect depends on the considered set-up. Thus, in the case of our experimental RFR, the distance of tubing required for conducting the gas from the reactor ends to the switching valves (Fig. 1) is low and the tube is 1/4″ O.D. Due to this fact, the volume of gas contained inside is negligible if compared with the volume of gas contained in the inert sections and the upper and lower dead volumes of the reactor, which are perfectly symmetric. The minimum amount of unconverted gas displaced from the reactor corresponds to a temperature profile that makes all the conversion to occur just after the gas enters in the catalytic section. The maximum amount corresponds to a temperature profile in which the all the conversion of the reactant occurs near of the bed end. The expressions for calculating the minimum and maximum volumetric fractions of the gas leaving the reactor without reacting are shown respectively in Eqs. (6) and (7), which are derived in the appendix.

$$(u_0 t_c)^{-1} \left(\frac{L - L_b}{2} + \varepsilon L_i \right) \tag{6}$$

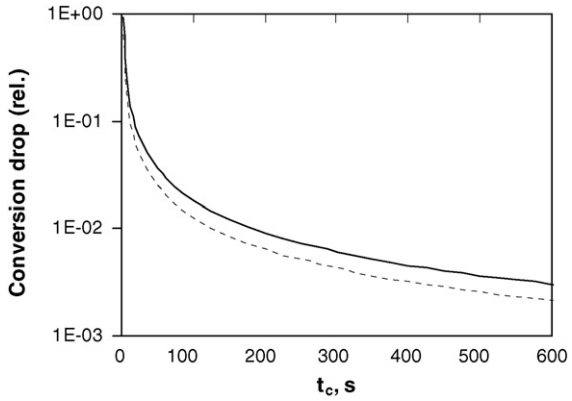

Fig. 5. Relative conversion drop due to *blow-up* effects. Conditions given in Table 1 ($u_0 = 0.155\ m\ s^{-1}$): *Minimum drop* (discontinuous line) and *maximum drop* (continuos line). Absolute conversion drop is obtained multiplying by the conversion in absence of this phenomenon.

$$(u_0 t_c)^{-1} \left(\frac{L + (2\varepsilon - 1)L_b}{2} - \varepsilon L_i \right) \quad (7)$$

These expressions allow calculating the intervals of relative conversion loss due to the *blow-up*. Applying them to the case of our experiments, we conclude that it is necessary to work with values of t_c above 100 s in order to avoid relative conversion drops higher than 2% (Fig. 5).

4.4. Validation of the results in the experimental rig

Experiments were carried out in order to verify the validity of the model regarding both the temperature profiles (particularly the maximum temperature in the catalytic bed) and conversions. The scope of these experiments was to compare the performance of both catalysts at the same operating conditions, but the expected workable regions do not superimpose at all for low values $y_{G,out,av}$, as previously indicated (Fig. 4). A direct comparison of the temperature profiles obtained experimentally does not provide useful information since these profiles were obtained at different conditions, namely at different values of $y_{G,0}$. Nevertheless, it is possible to compare the PSS temperature profile shapes by using the relative temperatures respect the $T_{S,max}$ of each profile, as represented in Fig. 6 for three different switching times (150 s, 300 s, and 600 s). These $T_{S,max}$ values, as well as the corresponding inlet methane concentration and the adiabatic temperature rise, are tabulated in Table 2. Obtained $T_{S,max}$ confirm that RFR have a behaviour adaptable to the activity of the catalyst being used, since the difference of $T_{S,max}$ between the two catalysts is about thrice higher than that due to the difference in ΔT_{ad} (27 °C) of the mixtures being fed. In other words, provided that $T_{S,0}$ and $y_{G,0}$ are high enough to make possible the auto-ignition, the RFR reaches a PSS state with a plateau temperature high enough to keep it ignited. It can be observed in Fig. 6 that the plateau is slightly wider for the metal oxides catalyst. This is due to its lower activity compared to the Pd one that makes the heat generation to be spreader throughout the catalytic section of the bed.

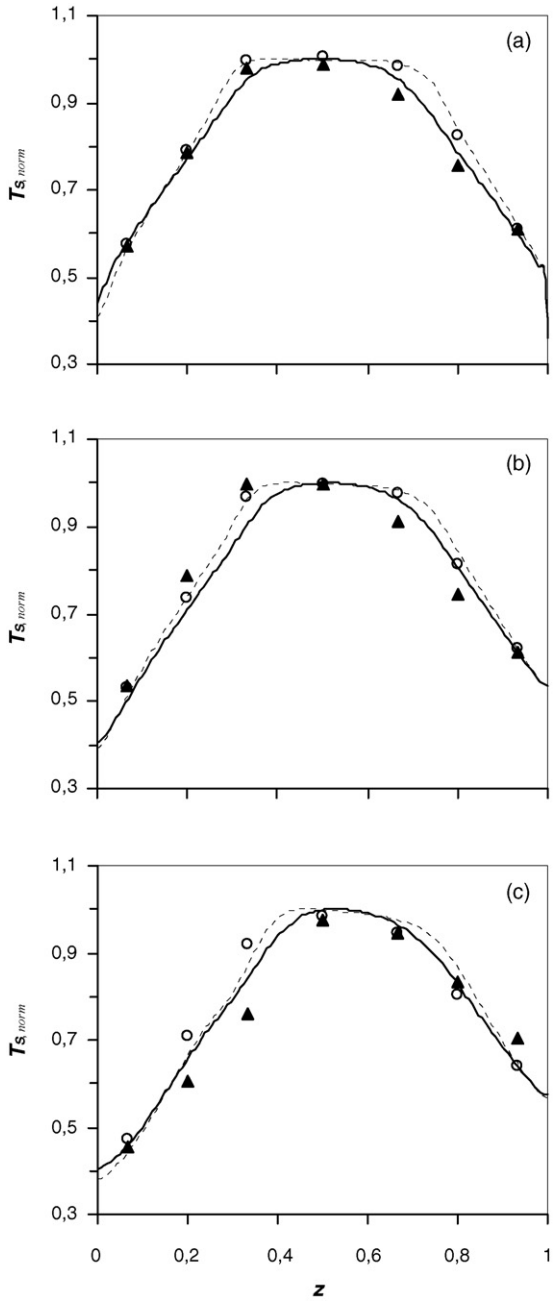

Fig. 6. Temperature profiles ($T_{S,rel}$) for three different t_c values ((a) 150s, (b) 300s, (c) 600). Metal oxides catalyst (discontinuous line for model predictions, (◯): for experimental); Pd catalyst (continuous line for model predictions, (▲): for experimental). Temperatures are normalised taking as reference the maximum temperatures for each catalyst and switching time (see Table 2).

Table 2
Maximum temperature (from the simulated profiles) for both catalysts at different t_c

t_c (s)	$T_{S,max}$ (K)	
	Pd ($\Delta T_{ad} = 67.5$ K)	Metal oxides ($\Delta T_{ad} = 94.5$ K)
150	759.7	847.6
300	767.0	845.0
600	756.5	852.6

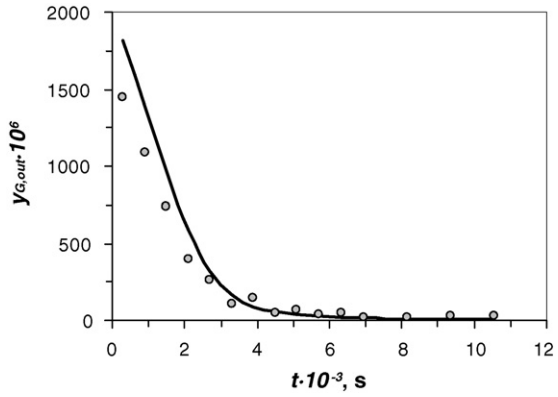

Fig. 7. Evolution of the outlet methane concentration ($y_{G,out}$) during the start-up for the metal oxides catalyst, $y_{G,0} = 3500$, $t_c = 600$s. Dots correspond to experimental data and continuous line corresponds to model predictions.

Full conversions were obtained at the PSS with both catalysts in experiments and simulations, but this is not enough to ensure the accuracy of the model. Proposed model must be also capable of predicting the behaviour of the reactor out of the full conversion zone. The preheating temperature for the Pd catalyst was high enough to obtain full conversion, not being possible to record experimental points at intermediate conversions at any moment of the experiment. Nevertheless, the preheating temperature used for the metal oxides catalyst allowed observing intermediate conversions at the beginning of the experiment. So, Fig. 7 shows the predicted and experimental evolution of outlet methane concentration during a start-up. It can be observed a good agreement of the proposed model with the experimental results, particularly in the time required to reach full conversion. Model presents slight positive deviations in the first minutes that decrease with time and become negligible when the evolution bends to a less steep decreasing of $y_{G,out}$. The gas sampling and analysis (GC) was done well after the flow reversal, approximately in the middle of the semi-cycle, so as to have a measurement of $y_{G,out}$ negligibly affected by the *blow-up*. This result is a further verification of the model and the experimental device performance regarding to that of Fig. 6, showing explicitly the validity of the parts of the model related to kinetics, mass transfer, and internal diffusion in the catalyst.

5. Conclusions

In this work, the type of catalyst has been shown to play a major role in the performance of a reverse-flow reactor carrying out the combustion of lean hydrocarbon mixtures, particularly of methane/air mixtures. Apart from the physical properties, which are similar for the catalysts used in this work, the most important catalytic properties regarding the influence on the RFR performance, and hence on the operating conditions to be fixed, are the catalytic activity, particularly its temperature dependence, and its resistance to thermal ageing. The two main groups of catalysts, noble metals and metal oxides, are opposite regarding these properties. The former are more active, but less thermal resistant than the latter.

It is worth to remark that the experimental results have confirmed the validity of the model in two important aspects: the PSS temperature profiles, particularly in the centre of the reactor, and the dynamic evolution of the methane concentration at the outlet during the start-up, thus supporting the conclusions drawn from simulations. The higher activity of noble metal catalysts confers them some advantages. The required preheating temperature is lower as well as the plateau temperature of the PSS. Therefore, the start-up is less energy-demanding and the driving force for the heat losses in the PSS is lower. Finally, self-maintained operation is possible with leaner mixtures when using the noble metal catalyst. Nevertheless, simulations have shown that the inlet concentration intervals at which the Pd catalyst can be operated are narrower due to its lower maximum allowable temperature. In general, it can be concluded that noble metal catalysts are more appropriate for leaner and stable, closely constant composition, mixtures, while metal oxides are more appropriate for richer mixtures, allowing concentration variations to some extent. The weaknesses of the noble metal based catalysts tend to disappear as their thermal resistance to deactivation is enhanced. Each little advance in this direction means an important improvement in the performance of RFR reactors applied to tail gases abatement.

Acknowledgements

This work has been financially supported by the European Commission (Contract ENV4-CT97-0599) and the Government of the Principality of Asturias through the research project ref. FC-03-PB02-133. Profs. Giancarlo Baldi, Antonello Barresi, Marco Vanni and Dr. Davide Fissore (*Politecnico di Torino*) are also gratefully acknowledged for their contributions in the modelling of the system and in the design of the experimental unit. Catalysts were a generous gift of Haldör-Topsøe (Lyngby, Denmark) and BASF (Barcelona, Spain).

Appendix A. Derivation of Eqs. (6) and (7).

The assumptions adopted in this derivation are exposed in the paragraph immediately above Eqs. (6) and (7). As in the model, pressure drop in the reactor is assumed to be negligible. The minimum and maximum possible relative conversion drop due to the *blow-up*, correspond to the minimum and maximum unconverted volume bypassed during a flow reversal respect the total of volume treated during a semi-cycle.

Total volume treated during a semi-cycle,

$$(u_0 t_c)\frac{\pi D_R^2}{4} \tag{A1}$$

The minimum bypassed unconverted gas volume corresponds to the most favourable case in which all the reactant is converted immediately after entering the catalytic section. This volume is the sum of the dead volume at one end of the reactor plus the void volume of one inert layer,

$$\frac{\pi D_R^2}{4}\left[\left(\frac{L - L_b}{2}\right) + \varepsilon L_i\right] \tag{A2}$$

The maximum bypassed unconverted volume corresponds to the least favourable case in which all the reactant is converted just at the end of the catalytic section. This volume is the minimum one (Eq. (A2)) plus the void volume of the catalytic section (Eq. (A3)),

$$\frac{\pi D_R^2}{4}(\varepsilon L_b - 2\varepsilon L_i) \quad \text{(A3)}$$

Eq. (6) is (A2)/(A1), whereas, Eq. (7) is (A2) + (A3)/A1.

References

[1] G.K. Boreskov, Y.S. Matros, Catal. Rev. Sci. Eng. 25 (1983) 551–590.
[2] Y.S. Matros, Catalytic Processes Under Unsteady-State Conditions, Elsevier Science Publishers B.V., Amsterdam, 1989.
[3] A.M. DeGroote, G.F. Froment, T. Kobylinski, Can. J. Chem. Eng. 74 (1996) 735–742.
[4] D. Neumann, M. Kirchhoff, G. Veser, Catal. Today 98 (2004) 565–574.
[5] R.Q. Ferreira, C.A. Costa, S. Masetti, Chem. Eng. Sci. 54 (1999) 4615–4627.
[6] J.D. Snyder, B. Subramaniam, Chem. Eng. Sci. 53 (1998) 727–734.
[7] Y.O. Jeong, D. Luss, Chem. Eng. Sci. 58 (2003) 1095–1102.
[8] T.N. Haynes, C. Georgakis, H.S. Caram, Chem. Eng. Sci. 47 (1992) 2927–2932.
[9] M.V. Annaland, R.C. Nijssen, Chem. Eng. Sci. 57 (2002) 4967–4985.
[10] M.S. Kulkarni, M.P. Dudukovic, AIChE J. 42 (1996) 2897–2910.
[11] Y.S. Matros, G.A. Bunimovich, Catal. Rev. Sci. Eng. 38 (1996) 1–68.
[12] S. Salomons, R.E. Hayes, M. Poirier, H. Sapoundjiev, Catal. Today 83 (2003) 59–69.
[13] S. Salomons, R.E. Hayes, M. Poirier, H. Sapoundjiev, Comput. Chem. Eng. 28 (2004) 1599–1610.
[14] U. Nieken, G. Kolios, G. Eigenberger, Catal. Today 20 (1994) 335–350.
[15] G. Eigenberger, U. Nieken, Int. Chem. Eng. 34 (1994) 4–16.
[16] M. Cittadini, M. Vanni, A.A. Barresi, G. Baldi, Chem. Eng. Sci. 56 (2001) 1443–1449.
[17] G. Eigenberger, U. Nieken, Chem. Eng. Sci. 43 (1988) 2109–2115.
[18] U. Nieken, G. Kolios, G. Eigenberger, Chem. Eng. Sci. 49 (1994) 5507–5518.
[19] B. Vandebeld, K.R. Westerterp, Chem. Eng. Technol. 17 (1994) 217–226.
[20] B. Vandebeld, K.R. Westerterp, AIChE J. 42 (1996) 1139–1148.
[21] C. Sapundzhiev, G.G. Grozev, D.G. Elenkov, Chem. Eng. Technol. 14 (1991) 209–212.
[22] J. Chaouki, C. Guy, C. Sapundzhiev, D. Kusohorsky, D. Klvana, Ind. Eng. Chem. Res. 33 (1994) 2957–2963.
[23] H. Sapoundjiev, J. Chaouki, C. Guy, D. Klvana, Chem. Eng. Commun. 125 (1993) 171–186.
[24] M. Cittadini, M. Vanni, A.A. Barresi, Chem. Eng. Process. 41 (2002) 437–443.
[25] A.A. Barresi, M. Vanni, AIChE J. 48 (2002) 648–652.
[26] P. Dufour, Y. Toure, Comput. Chem. Eng. 28 (2004) 2259–2270.
[27] D. Edouard, P. Dufour, H. Hammouri, Comput. Chem. Eng. 29 (2005) 851–865.
[28] F.L. Chan, J.M. Keith, J. Environ. Manage. 78 (2006) 223–231.
[29] K. Gosiewski, Chem. Eng. J. 107 (2005) 19–25.
[30] D. Fissore, A.A. Barresi, G. Baldi, M.A.G. Hevia, S. Ordonez, F.V. Diez, AIChE J. 51 (2005) 1654–1664.
[31] M.A.G. Hevia, S. Ordóñez, F.V. Díez, AIChE J. 52 (2006) 3203–3209.
[32] M.A.G. Hevia, S. Ordoñez, F.V. Diez, D. Fissore, A.A. Barresi, AIChE J. 51 (2005) 3020–3027.
[33] P. Marin, M.A.G. Hevia, S. Ordonez, F.V. Diez, Catal. Today 105 (2005) 701–708.
[34] D. Fissore, A.A. Barresi, Chem. Eng. Res. Des. 81 (2003) 611–617.
[35] P. Hurtado, S. Ordóñez, A. Vega, F.V. Díez, Chemosphere 55 (2004) 681–689.
[36] A.C. Hindmarsh, ODEPACK, a Systematized Collection of ODE Solvers, North Holland, Amsterdam, 1983.
[37] F. Diez, A. Vega, S. Ordóñez, M.A.G. Hevia, D. Fissore, M. Cittadini, M. Vanni, A. Barresi, G. Baldi, Dispositivo para el control de flujo de calor a través de la pared en equipos pequeños, Patent 2,239,542 (Spain) (2005).
[38] S. Ordonez, L. Bello, H. Sastre, R. Rosal, F.V. Diez, Appl. Catal. B: Environ. 38 (2002) 139–149.
[39] M.A.G. Hevia, Catalytic combustion of methane in reverse flow reactors: design, operation and simulation, PhD Thesis, Universidad de Oviedo (Spain) (2004).
[40] S. Yang, A. Maroto-Valiente, M. Benito-González, I. Rodríguez-Ramos, A. Guerrero-Ruiz, Appl. Catal. B: Environ. 28 (2000) 223–233.
[41] S.A. Velardi, A.A. Barresi, Chem. Eng. Sci. 57 (2002) 2995–3004.
[42] K.M. VandenBussche, G.F. Froment, Can. J. Chem. Eng. 74 (1996) 729–734.